Progress In Electromagnetics Research Letters, Vol. 100, 81–89, 2021

Synthesis of a Dual-Band Flat-Top Pattern Using Polarization Dependent Metasurface

Pallapati Vinod Kumar* **and Basudeb Ghosh**

Abstract—A simple and novel polarization-dependent phase gradient metasurface (PGMS) is proposed to synthesize a flat-top radiation pattern by dividing the metasurface (MTS) into multiple regions. Each sub-region generates a beam in a particular direction, and multiple beams with different directions form a flat-top pattern in the far-field. A flat-top pattern in a single and 3D plane is realized by dividing the MTS into two and four regions, respectively. The proposed MTS consists of a multi-layered elliptical geometry encircled by a square loop. The elliptical shape of the unitcell offers polarization-dependent behavior and produces dual-band characteristics for different incident wave polarizations at 10 and 12 GHz. Two microstrip patch antennas operating at 10 GHz and 12 GHz are placed at the focal point of the MTS. The simulated flat-top beamwidths in a single plane with a 1 dB ripple are 36° and 34° at 10 and 11.8 GHz, respectively. Similarly, in 3D space, the beamwidths are 33° and 31° at 10 and 11.8 GHz, respectively. Both simulated and measured results are presented for 3D flat-top patterns.

1. INTRODUCTION

The flat-top radiation pattern has uniform gain over a wide angular region with low ripples, usually less than 1 dB. Hence, the antennas with a flat pattern have been used in modern communication systems to serve uniform signal strength within the desired coverage area. Adaptive phased array antennas can provide flat-top radiation patterns by controlling the amplitude and phase of the individual antenna elements [1–4]. The amplitude and phases of the antenna elements are synthesized using various optimization algorithms. However, this approach suffers from its narrow bandwidth and the requirement of a complex feeding network. Alternatively, the flat-top pattern is also generated by shaping the reflector and lens profile as demonstrated in [5–8]. However, lenses and reflectors at microwave frequencies suffer from their bulky size and heavy weight. On the other hand, PGMS eliminates the feeding network requirement, thereby reducing the weight and complexity of the overall antenna system.

Over the past decade, metasurfaces are also found in several applications such as mutual coupling reduction, polarization conversion, and bandwidth enhancement [9–11]. Among metasurfaces, PGMS antennas have received attention from researchers due to their localized phase characteristics and easy fabrication. These MTSs have found applications in gain enhancement and beam shaping at microwave [12–16] and millimeter-wave frequencies [17, 18]. Recently, flat-top radiation pattern using MTS is presented in [19–21]. Multiple PGMSs separated by an optimized distance result in a flat-top radiation pattern [19]. On the other hand, the transmission characteristics of the unitcells were optimized using the array theory for flat-top pattern beam shaping [20, 21].

Most of the literature concentrates on the design of single-band flat-top pattern synthesis. Multi-band PGMS antennas offer alternate solutions to traditional multi-band antennas with reduced cost and enhanced bandwidth. Several multi-band PGMS antennas are reported in [22–24]. The unitcell design

Received 4 July 2021, Accepted 19 September 2021, Scheduled 1 October 2021
* Corresponding author: Pallapati Vinod Kumar (vinodkumar.iist@gmail.com).
The authors are with the Indian Institute of Space Science and Technology, India.

for multi-band operation is challenging, requiring a high transmission/reflection coefficient with phase controllability [25–28]. However, dual-band operation can also be achieved by asymmetric unitcells, which can provide independently controllable characteristics for different polarizations of the incident wave [29, 30]. Hence, an elliptical unitcell is considered, whose phase characteristics for x- and y-polarizations can be controlled independently by varying the major (a) and minor (b) axes, respectively.

In this paper, a novel technique is proposed to realize a dual-band flat-top radiation pattern. The novelty of the present design lies in the synthesis procedure, where the entire MTS is divided into multiple subregions. Each subregion is designed to tilt the beam in an optimized direction. The beams from multiple regions result in a flat-top pattern. Hence, the challenges of simultaneous amplitude and phase control can be effectively avoided. Another significant contribution of this work is the realization of a flat-top beam at two frequencies, which is obtained by the elliptical shape of the unitcell. Initially, the MTS is divided into two subregions as shown in Fig. 1(a), to produce a flat-top pattern in the xz-plane. Then, the work is further carried out in 3D space by dividing the entire MTS into four subregions, as shown in Fig 1(b). These MTSs are referred to as MTS-1 and MTS-2. Some preliminary results based on the present work are presented in [31]. This paper is organized as follows. The design principle to realize flat-top radiation pattern is presented in Section 2. The unitcell design and analysis are presented in Section 3. Section 4 presents the simulation and measured parameters of the antennas with MTS. Finally, the conclusions are outlined in Section 5.

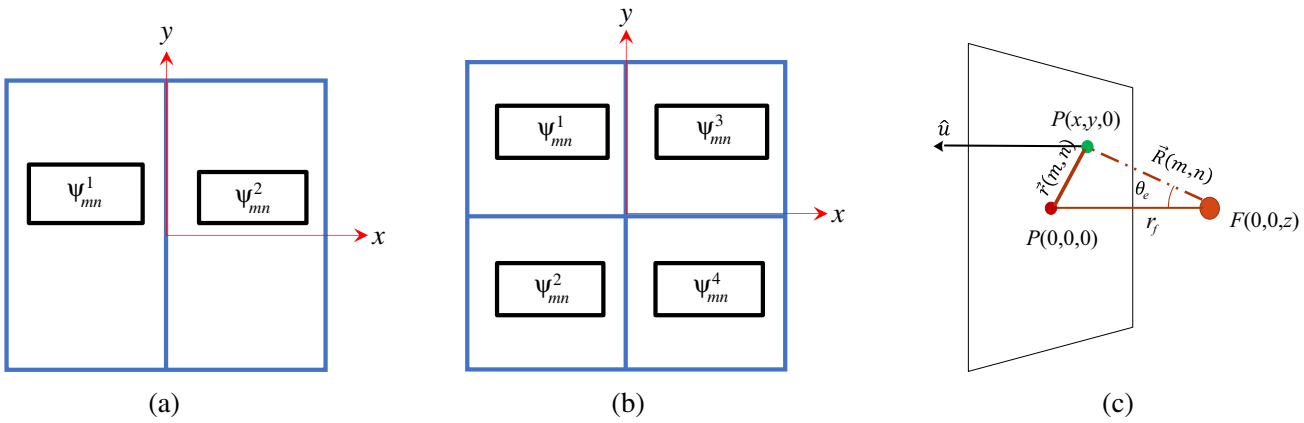

Figure 1. Flat-top pattern generation with MTS by dividing into (a) two sub-regions (MTS-1), (b) four sub-regions (MTS-2), (c) alignment of the MTS and antenna.

2. WORKING PRINCIPLE

The principle of flat-top pattern synthesis for dual-band operation is presented here. The radiation pattern of a 2D planar array with $M \times N$ elements for the MTS and antenna configuration is shown in Fig. 1(c) and is given by [27]

$$E(\theta,\phi) = \sum_{m=-M/2}^{M/2} \sum_{n=-N/2}^{N/2} \frac{\cos^{qe}(\theta,\phi) \cdot \cos^{qf}(\theta,\phi)_{mn}}{|\overrightarrow{r}_{mn} - \overrightarrow{r_f}|} |T_{mn}| \cdot e^{-jk(|\overrightarrow{r}_{mn} - \overrightarrow{r_f}| - \overrightarrow{r}_{mn} \cdot \hat{u})} \cdot e^{\psi_{mn}} \tag{1}$$

where k is the wavenumber, $\overrightarrow{r}_{mn}$ the position vector of mnth element, $\overrightarrow{r_f}$ the feed position vector, and $\cos^{qf}(\theta,\phi)_{m,n}$ the approximation of amplitude (for patch antenna $qf \approx 1.2$) due to the feed at (m,n)th position. Here, $(\theta,\phi)_{mn}$ is the angle between feed and the mnth element. $\cos^{qe}(\theta,\phi)e^{(jk\overrightarrow{r}_{mn}\cdot\hat{u})}$ is the element pattern of the unitcell, and $|T_{mn}|$ is the transmission coefficient of the PGMS at (m,n)th position. The main beam direction is represented by $\hat{u}$, and ψ_{mn} is the compensated phase on the MTS given by [27]

$$\psi_{mn} = jk\left(|\overrightarrow{r}_{mn} - r_f| - \overrightarrow{r}_{mn} \cdot \hat{u}\right) + \psi_0 \tag{2}$$

where ψ_0 is the phase reference located at the center of MTS.

As shown in Fig. 1(a), MTS-1 is divided into two regions with phase profiles ψ^1_{mn} and ψ^2_{mn} to generate two beams simultaneously in $\hat{u}_1(\theta = \theta_1, \phi = 0°)$ and $\hat{u}_2(\theta = \theta_1, \phi = 180°)$ directions. By proper optimization of the angle θ_1, a flat-top radiation pattern in $\phi = 0°$ plane can be realized. Similarly, MTS-2 generates four beams simultaneously at $(\theta = \theta_2)$ with $\phi = 45°, 135°, 225°, 315°$ directions. Optimization of θ_2 results into a 3D flat-top pattern.

A 15×15 array with unitcell periodicity of 9 mm and feed position (F) at 30 mm away from the center of MTS is considered in this work. The phase at the center of MTS is considered as $\psi_0 = 0°$. Using Eq. (2), ψ^1_{mn} and ψ^2_{mn} are calculated for an initial value of $\theta_1 = 15°$. The resulting radiation pattern for the complete MTS is obtained through Eq. (1). To obtain a nearly flat-top pattern, the value of θ_1 is varied, and at each step the resulting radiation pattern is calculated. It is found that a nearly flat-top pattern is obtained for $\theta_1 = 20°$. The corresponding phase profiles for 10 GHz and 12 GHz are shown in Figs. 2(a) and 2(b), respectively. Similarly, for 3D flat-top pattern, the optimized value of θ_2 is 23°. The resulting phase profiles are depicted in Figs. 2(c) and 2(d) for 10 GHz and 12 GHz, respectively. The flat-top beamwidth can be varied by changing the MTS dimension and focal distance.

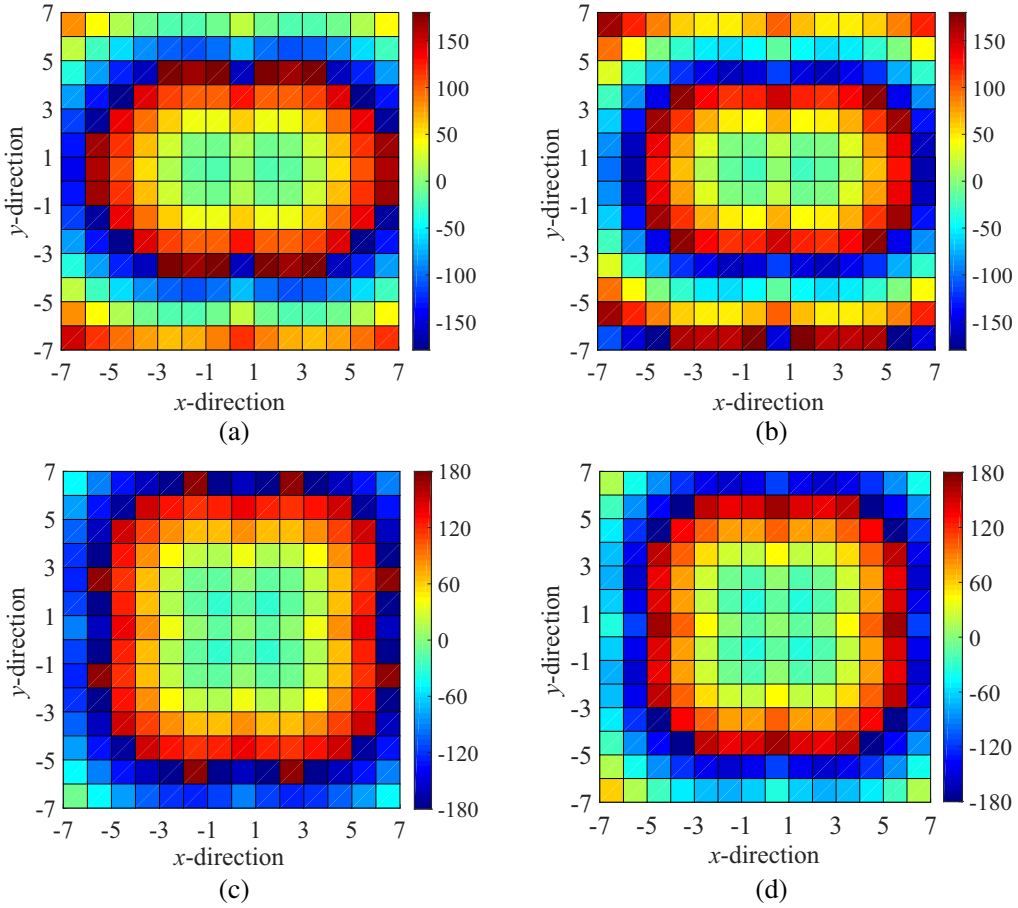

Figure 2. Phase profile for the MTS: Single plane at (a) 10 GHz, (b) 12 GHz; 3-D plane at (c) 10 GHz and (d) 12 GHz.

3. UNIT CELL DESIGN AND ANALYSIS

For proper functioning of MTS, the unitcell should provide a complete 360° phase coverage. The phase coverage at a given frequency can be increased by adding more dielectric layers, and a minimum of

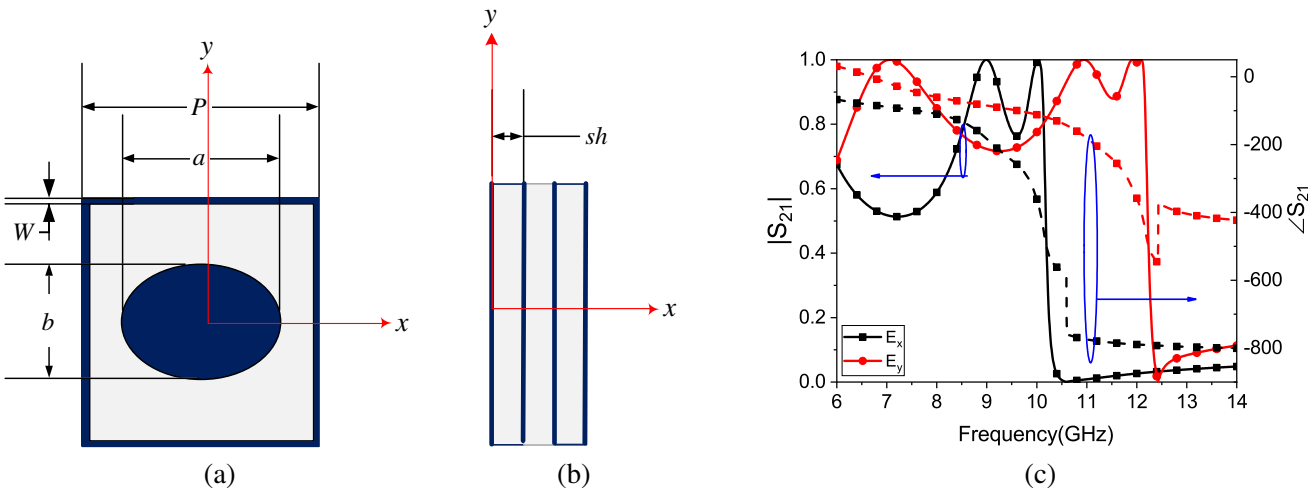

Figure 3. Unitcell dimensions (mm) are given as $P = 9$, $w = 0.2$, $sh = 0.8$, $a = 8$, $b = 6.5$: (a) top view, (b) side view; (c) variation of transmission coefficient for x and y-polarized waves.

three layers are required for 360° phase coverage [27]. The proposed unitcell consists of four identical elliptical patches encircled by a square loop printed on a three-layer dielectric substrate (FR4, $\epsilon_4 = 4.4$), and the top and side views of the unitcell are depicted in Figs. 3(a) and 3(b), respectively. The unitcell analysis is carried out in CST Microwave Studio with unitcell boundary conditions placed along x- and y-directions and excited with Floquet ports along $\pm z$-directions. The unitcell is illuminated with two orthogonal Floquet modes. Fig. 3(c) shows the transmission response of the unitcell in the frequency range of [6–14] GHz. For E_x incidence, it can be seen that $|S_{21}|$ is greater than 0.7 in the frequency range from 8 to 10.1 GHz with phase variation of 350°. Similarly, for E_y incidence, $|S_{21}|$ is greater than 0.75 in the frequency range from 10 to 12.2 GHz with phase variation of 450°. The $|S_{21}|$ drops significantly beyond 10.2 GHz and 12.2 GHz for x and y polarized incident waves, respectively.

To realize 360° phase variation at 10 GHz, a is varied from 4 to 8 mm with an interval of 0.02 mm for a fixed value of $b = 6.5$ mm. Similarly, b is varied from 2 to 6.5 mm with $a = 8$ mm. Fig. 4(a) shows the variation of transmission response at 10 and 12 GHz for E_x and E_y incidences, respectively. It can be seen that $|S_{21}|$ is always greater than 0.65 with phase varying from $-40°$ to $-380°$. Hence, at 10 GHz, a stable amplitude with a phase span of 340° is achieved. Also, the effect of a variation at 12 GHz for y-polarized wave is minimum. Similarly, for b variation at 12 GHz, $|S_{21}|$ is greater than 0.7 with 370° phase variation for E_y incidence as shown in Fig. 4(b).

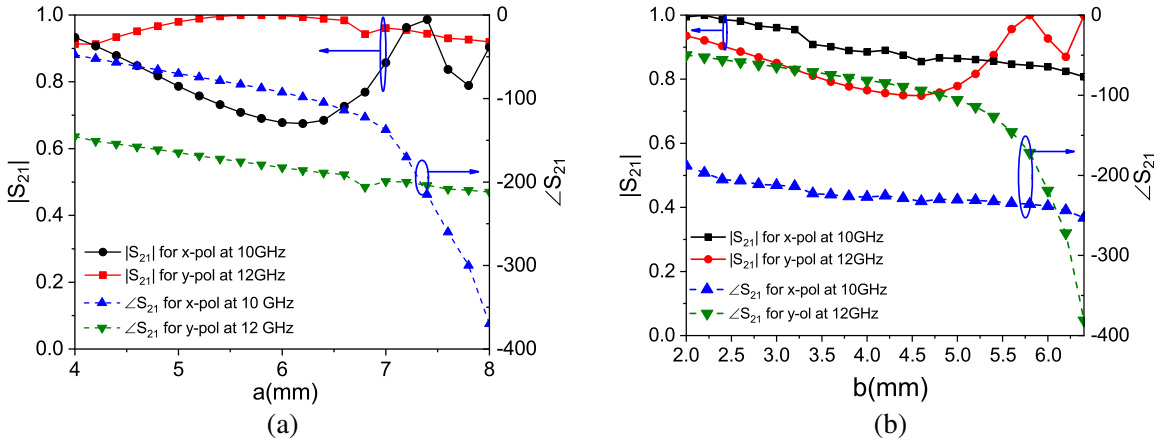

Figure 4. Simulated unitcell response: (a) a variation with $b = 6.5$ mm, (b) b variation with $a = 8$ mm.

4. METASURFACE DESIGN AND ANALYSIS

The MTS is independently designed by one-to-one phase mapping with corresponding dimensions of a at 10 GHz and b at 12 GHz. The designed MTSs for 2D and 3D flat-top pattern generation are shown in Figs. 5(a) and 5(b), respectively. For the analysis of the MTS, a dual-band antenna with broadside radiation pattern having orthogonal polarization purity needs to be placed at the focal point. A dual-band patch antenna with orthogonal polarization may be designed to demonstrate the performance of the MTS. However, the primary concern of the current study is to realize a dual-band flat-top radiation pattern. For simplicity, we have demonstrated the performance of MTS by two independent patch antennas operating at two operating frequencies. Hence, two linearly polarized coaxial fed patch antennas printed on an FR4 substrate ($\epsilon_r = 4.4$, thickness = 1.6 mm) operating at 10 GHz and 12 GHz are considered for the realization as shown in Fig. 6(a), and they are referred to as antenna-1 and antenna-2. The antenna dimensions are reported in Table 1. The antennas with and without MTS are analyzed in CST Microwave Studio using T-solver with open and add space boundary conditions in all directions. Antenna-1 with and without MTS is analyzed from 9 GHz to 10.5 GHz; however, antenna-2 with and without MTS is analyzed from 11 GHz to 12.5 GHz. It is observed that a single standalone patch antenna has typical gains of 4.2 dB and 4.6 dB at 10 and 12 GHz, respectively.

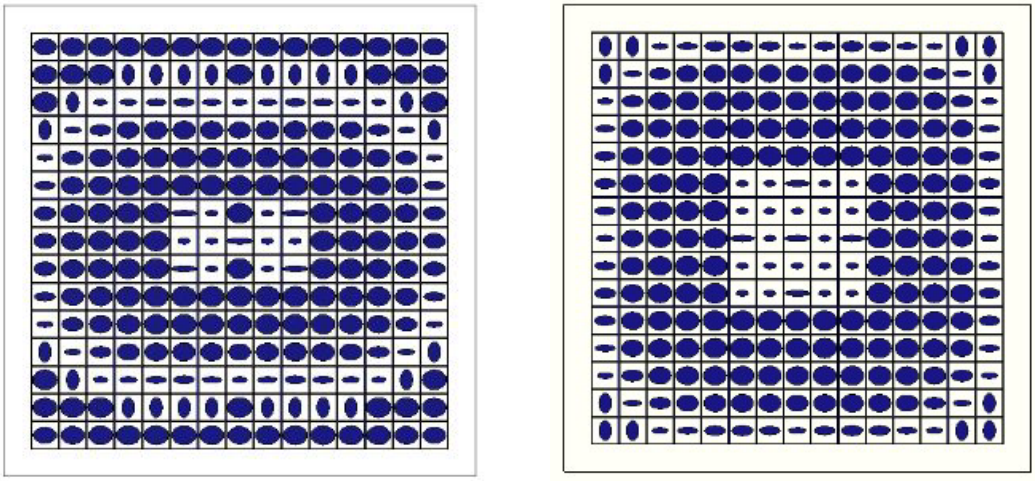

(a) (b)

Figure 5. Designed PGMS (a) MTS-1, (b) MTS-2.

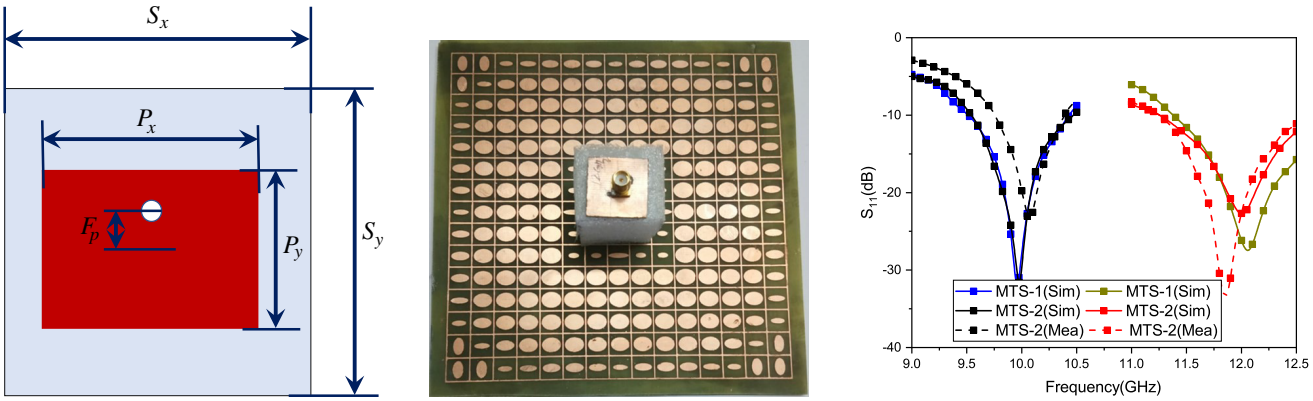

(a) (b) (c)

Figure 6. Antenna with MTS-2: (a) antenna, (b) fabricated prototype, (c) reflection coefficient.

Table 1. Dimensions of the patch antennas (all dimensions are in mm).

Antenna	S_x	S_y	P_x	P_y	F_p
Antenna-1	15	15	7	6.25	1.6
Antenna-2	15	15	6	5	1.4

At 10 GHz for E_x excitation on MTS, antenna-1 radiating edge is placed along the x-direction. Similarly, for antenna-2, the radiating edge is placed along y direction to excite E_y on MTS. As the patch antenna is not an ideal point source, the phase center is not precisely located 30 mm away from the center of MTS. Hence, the focal distance is optimized, and for $F = 40$ mm, a flat-top pattern with ripples less than 1 dB is realized. Fig. 6(c) shows the simulated reflection coefficient of the antenna with MTS-1 and MTS-2.

For MTS-1, the simulation results show a good impedance matching with a flat-top pattern at 10 GHz and 11.8 GHz. At 10 GHz, a peak gain of 9 dB with -30 dB cross-pol level has been observed. Fig. 7(a) shows the radiation pattern at 10 GHz. It is evident that in $\phi = 0^\circ$ plane, a flat-top pattern is generated with a 1 dB ripple bandwidth of 36°. In $\phi = 90^\circ$ plane, the beam is in the broadside direction as expected. The side-lobe levels (SLLs) of -10 and -11 dB have been observed in $\phi = 0^\circ$ and $\phi = 90^\circ$ planes, respectively. Similarly at 11.8 GHz, 1 dB ripple width of 34° has been observed in $\phi = 0^\circ$ plane as shown in Fig. 7(b). A peak gain of 11 dB with SLLs of -11 dB and -10 dB have been observed in $\phi = 0^\circ$ and $\phi = 90^\circ$ planes, respectively.

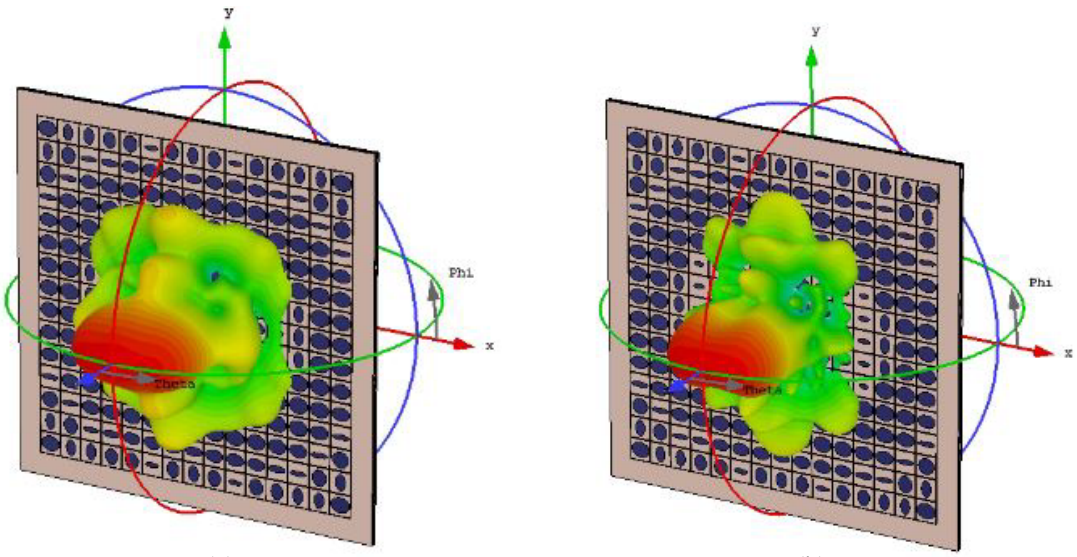

(a) (b)

Figure 7. Simulated radiation pattern of the antenna with MTS-1 at (a) 10 GHz, (b) 11.8 GHz.

Figure 6(b) shows the fabricated structure of MTS-2 using a chemical etching process having an accuracy of 0.1 mm. The antenna and metasurface are fabricated using chemical etching procedure. The antenna input characteristics are measured using a PNA. The radiation patterns are measured with a horn antenna. Due to the non-availability of anechoic chamber, the radiation pattern is measured in an open environment. The simulated and measured reflection coefficients with antenna-1 and antenna-2 are shown in Fig. 6(c), where a foam of 40 mm is used between MTS and antenna. A very small difference in the reflection coefficient (S_{11}) is observed due to the fabrication tolerance of the MTS and antenna, however the maximum deviation is observed to be 1.5% and 1.6% at 10 GHz and 12 GHz, respectively. The simulated and measured radiation patterns of the MTS for both the frequencies are shown in Fig. 8. For pattern and gain measurement, X-band horn antennas have been used as reference antennas. The

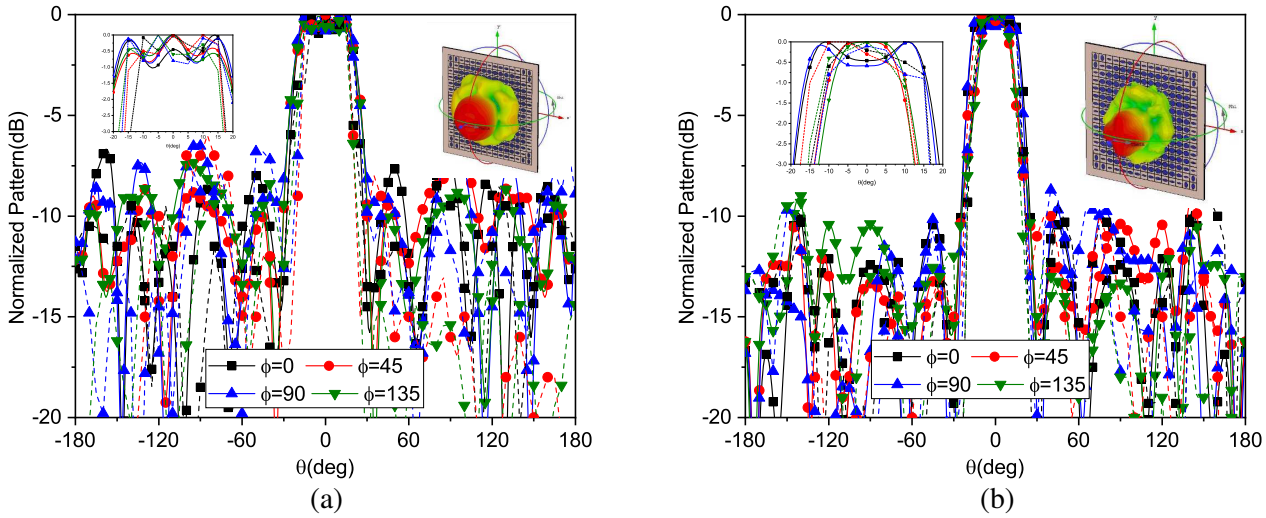

Figure 8. Far-field patterns of the antenna with MTS-2 (simulated-straight line, measured-dotted line, 3D-radiation pattern is shown in the inset) at (a) 10 GHz, (b) 11.8 GHz.

results show a flat-top pattern with ripples less than 1 dB in the frequency range of 9.8 to 10 GHz for x-polarized incident wave and 11.6 to 11.8 GHz for y-polarized incident wave. However, the maximum 1 dB ripple beamwidth is observed at 10 GHz and 11.8 GHz. It can also be seen that in all the planes, the 1 dB ripple beamwidth of 30° is achieved with the measured gain of 7.8 dB. Similarly at 11.8 GHz, 1 dB ripple beamwidth of 26° has been achieved with the gain of 9.1 dB. The simulated efficiency of the system is about 57% at 10 and 11.8 GHz, which is a moderate value for MTS-antennas. However, SLLs and the back lobe levels are only −10 dB and −12 dB, respectively. Higher SLL appears because of the non-uniformity of transmission amplitude throughout the MTS. The proposed method offers stable radiation characteristics, gain, and beamwidth at both operating frequencies. The beamwidth can be enhanced by reducing the MTS dimensions. A comparison of the present work with the earlier works on flat-top radiation patterns is given in Table 2.

Table 2. Comparison table with other works.

	[3]	[32]	[20]	[21]	[19]	Proposed structure
Method	Antenna array	Lens	MTS	MTS	MTS	MTS
Center frequency (GHz)	1.7	28	10	10	10	10/12
Beamwidth (1 dB)	40°	60°	80°	76°	34°	30°/26°
Gain (dB)			-	-	14.8	7.8/9.1
Number of elements			676	169	162	225
Number of antennas	10	1	1	1	1	1/1
Size (λ^2)	1×7.9	7.5×7.5	4.8×4.8	4.3×4.3	4×4	4.5×4.5

5. CONCLUSION

A dual-band polarization-dependent PGMS is designed to generate flat-top patterns in single and dual planes. The MTS is divided into two and four subregions to generate a flat-top pattern in single and dual planes, respectively. For demonstration, a 15×15 PGMS is designed occupying $135 \times 135\,\text{mm}^2$ with a focal point of 30 mm. The MTS is excited with antennas operating at 10 GHz and 12 GHz for E_x

and E_y polarizations, respectively. The proposed method is very simple, and it can be easily fabricated. A good matching between the simulation and measurement is achieved. The present work suffers from high SLL, which can be reduced by reducing the quantization error in amplitude and phase. Further, it can be reduced by introducing amplitude tapering over the MTS.

REFERENCES

1. Mailloux, R. J., *Phased Array Antenna Handbook*, Artech House, 2017.
2. Volakis, J. L., *Antenna Engineering Handbook*, McGraw-Hill Education, 2007.
3. Zhou, H.-J., Y.-H. Huang, B.-H. Sun, and Q.-Z. Liu, "Design and realization of a flat-top shaped beam antenna array," *Progress In Electromagnetics Research Letters*, Vol. 5, 159–166, 2008.
4. Monavar, F. M., S. Shamsinejad, R. Mirzavand, J. Melzer, and P. Mousavi, "Beam-steering SIW leaky-wave subarray with flat-topped footprint for 5G applications," *IEEE Transactions on Antennas and Propagation*, Vol. 65, No. 3, 1108–1120, 2017.
5. Rao, S., L. Shafai, and S. K. Sharma, *Handbook of Reflector Antennas and Feed Systems Volume III: Applications of Reflectors*, Artech House, 2013.
6. Nguyen, N. T., R. Sauleau, and L. Le Coq, "Lens antennas with flat-top radiation patterns: Benchmark of beam shaping techniques at the feed array level and lens shape level," *2009 3rd European Conference on Antennas and Propagation*, 2834–2837, 2009.
7. Chahat, N., E. Decrossas, D. Gonzalez-Ovejero, O. Yurduseven, M. J. Radway, R. E. Hodges, P. Estabrook, J. D. Baker, D. J. Bell, T. A. Cwik, et al., "Advanced cubesat antennas for deep space and earth science missions: A review," *IEEE Antennas and Propagation Magazine*, Vol. 61, No. 5, 37–46, 2019.
8. Chen, C., B. Zhang, and K. Huang, "Nonuniform Fabry-Perot leaky-wave antenna with flat-topped radiation patterns for microwave wireless power transmission," *IEEE Antennas and Wireless Propagation Letters*, Vol. 18, No. 9, 1863–1867, 2019.
9. Ozdemir, E., O. Akgol, F. Ozkan Alkurt, M. Karaaslan, Y. I. Abdulkarim, and L. Deng, "Mutual coupling reduction of cross-dipole antenna for base stations by using a neural network approach," *Applied Sciences*, Vol. 10, No. 1, 378, 2020.
10. Öztürk, M., U. K. Sevim, O. Altıntaş, E. Ünal, O. Akgöl, M. Karaaslan, and C. Sabah, "Design of a linear to circular polarization converter integrated into a concrete construction for radome applications," *International Journal of Microwave and Wireless Technologies*, 1–8, 2021.
11. Abdulkarim, Y. I., H. N. Awl, F. F. Muhammadsharif, M. Karaaslan, R. H. Mahmud, S. O. Hasan, Ö. Işık, H. Luo, and S. Huang, "A low-profile antenna based on single-layer metasurface for Ku-band applications," *International Journal of Antennas and Propagation*, Vol. 2020, 2020.
12. Yu, N., P. Genevet, M. A. Kats, F. Aieta, J.-P. Tetienne, F. Capasso, and Z. Gaburro, "Light propagation with phase discontinuities: Generalized laws of reflection and refraction," *Science*, Vol. 334, No. 6054, 333–337, 2011.
13. Ding, F., A. Pors, and S. I. Bozhevolnyi, "Gradient metasurfaces: A review of fundamentals and applications," *Reports on Progress in Physics*, Vol. 81, No. 2, 026401, 2017.
14. Faenzi, M., D. Gonzalez-Ovejero, and S. Maci, "Flat gain broadband metasurface antennas," *IEEE Transactions on Antennas and Propagation*, Vol. 69, No. 4, 1942–1951, 2020.
15. He, B., J. Fan, Y. Cheng, F. Chen, H. Luo, and R. Gong, "Thermally tunable terahertz vortex beam generator based on an insb metasurface," *JOSA B*, Vol. 38, No. 5, 1518–1524, 2021.
16. Zhou, E., Y. Cheng, F. Chen, and H. Luo, "Wideband and high-gain patch antenna with reflective focusing metasurface," *AEU-International Journal of Electronics and Communications*, Vol. 134, 153709, 2021.
17. Fan, J. and Y. Cheng, "Broadband high-efficiency cross-polarization conversion and multi-functional wavefront manipulation based on chiral structure metasurface for terahertz wave," *Journal of Physics D: Applied Physics*, Vol. 53, No. 2, 025109, 2019.

18. Wang, J., J. Fan, H. Shu, C. Liu, and Y. Cheng, "Efficiency-tunable terahertz focusing lens based on graphene metasurface," *Opto-Electronic Engineering*, Vol. 48, No. 4, 200319-1, 2021.
19. Singh, A. K., M. P. Abegaonkar, and S. K. Koul, "Wide angle beam steerable high gain flat top beam antenna using graded index metasurface lens," *IEEE Transactions on Antennas and Propagation*, Vol. 67, No. 10, 6334–6343, 2019.
20. Li, H., G. Wang, T. Cai, H. Hou, and W. Guo, "Wideband transparent beam-forming metadevice with amplitude-and phase-controlled metasurface," *Physical Review Applied*, Vol. 11, No. 1, 014043, 2019.
21. Li, H., G. Wang, L. Zhu, X. Gao, and H. Hou, "Wideband beam-forming metasurface with simultaneous phase and amplitude modulation," *Optics Communications*, Vol. 466, 124601, 2020.
22. Li, H.-P., G.-M. Wang, X.-J. Gao, J.-G. Liang, and H.-S. Hou, "An X/Ku-band focusing anisotropic metasurface for low cross-polarization lens antenna application," *Progress In Electromagnetics Research*, Vol. 159, 79–91, 2017.
23. Cai, T., G.-M. Wang, J.-G. Liang, Y.-Q. Zhuang, and T.-J. Li, "High-performance transmissive meta-surface for C-/X-band lens antenna application," *IEEE Transactions on Antennas and Propagation*, Vol. 65, No. 7, 3598–3606, 2017.
24. Zhao, R., L. Huang, and Y. Wang, "Recent advances in multi-dimensional metasurfaces holographic technologies," *PhotoniX*, Vol. 1, No. 1, 1–24, 2020.
25. Ryan, C. G., M. R. Chaharmir, J. Shaker, J. R. Bray, Y. M. Antar, and A. Ittipiboon, "A wideband transmitarray using dual-resonant double square rings," *IEEE Transactions on Antennas and Propagation*, Vol. 58, No. 5, 1486–1493, 2010.
26. Li, H., G. Wang, H.-X. Xu, T. Cai, and J. Liang, "X-band phase-gradient metasurface for high-gain lens antenna application," *IEEE Transactions on Antennas and Propagation*, Vol. 63, No. 11, 5144–5149, 2015.
27. Abdelrahman, A. H., F. Yang, A. Z. Elsherbeni, and P. Nayeri, "Analysis and design of transmitarray antennas," *Synthesis Lectures on Antennas*, Vol. 6, No. 1, 1–175, 2017.
28. Fan, J., Y. Cheng, and B. He, "High-efficiency ultrathin terahertz geometric metasurface for fullspace wavefront manipulation at two frequencies," *Journal of Physics D: Applied Physics*, Vol. 54, No. 11, 115101, 2021.
29. Jia, S. L., X. Wan, D. Bao, Y. J. Zhao, and T. J. Cui, "Independent controls of orthogonally polarized transmitted waves using a huygens metasurface," *Laser & Photonics Reviews*, Vol. 9, No. 5, 545–553, 2015.
30. Ma, H. F., G. Z. Wang, G. S. Kong, and T. J. Cui, "Independent controls of differently-polarized reflected waves by anisotropic metasurfaces," *Scientific Reports*, Vol. 5, 9605, 2015.
31. Kumar, V. and B. Ghosh, "Dual-band flat-top pattern synthesis using phase gradient metasurface," *2020 International Symposium on Antennas & Propagation (APSYM)*, 105–108, IEEE, 2020.
32. Maximidis, R., A. Smolders, G. Toso, and D. Caratelli, "Planar reactively loaded array antenna with flat-top radiation pattern characteristics," 2020 *IEEE International Symposium on Antennas and Propagation and North American Radio Science Meeting*, 2091–2092, IEEE, 2020.